

Interplay between Jahn-Teller distortions and structural degrees of freedom in pseudocubic states in manganite perovskites

Ben R. M. Tragheim¹,¹ Elodie A. Harbourne,² Clemens Ritter³,³ Andrew L. Goodwin²,² and Mark S. Senn^{1,*}

¹Department of Chemistry, University of Warwick, Gibbet Hill, Coventry CV4 7AL, United Kingdom

²Department of Chemistry, Inorganic Chemistry Laboratory, University of Oxford, South Parks Road, Oxford OX1 3QR, United Kingdom

³Institut Laue-Langevin, 71 Avenue des Martyrs, CS20156, 38042 Grenoble Cédex 9, France



(Received 16 April 2025; revised 9 July 2025; accepted 27 August 2025; published 9 September 2025)

The average structure of the solid solution $\text{LaMn}_{1-x}\text{Ga}_x\text{O}_3$ (LMGO) has been investigated from a symmetry-motivated approach utilizing synchrotron x-ray and neutron powder diffraction techniques. We show experimentally that a trilinear coupling term ($\Gamma_5^+M_2^+M_3^+$) between shear strain, octahedral rotation, and the C-type orbital ordering mode is responsible for driving the orthorhombic to pseudocubic phase transition occurring in the composition range $0.5 < x < 0.6$. Our Monte Carlo simulations elucidate the macroscopic origin of this coupling to shear strain, and point to its importance with respect to controlling the orbital order-disorder transitions. We find that the emergence of the pseudocubic state can be rationalized by considering the competition between this trilinear term and a linear-quadratic term of the out-of-phase octahedral tilting with strain ($\Gamma_5^+(R_5^-)^2$). Illustrating the general nature of these results, we construct a simple function that captures the change in Landau free energy at the order-disorder transition, in parameters that are trivial to relate to the concentration of Jahn-Teller active species, temperature, tolerance factor, and unit cell strain, for a broad range of manganite perovskites. Our results point to the fact that far from the pseudocubic state being a symptom of orbital disorder, in many cases, it is more correctly to view it as a cause. The results have a broad impact on the study of orbital ordering physics in the perovskite materials and on chemical and physical control parameters through which to tune the richness of the intertwined physical properties.

DOI: [10.1103/cj28-2swm](https://doi.org/10.1103/cj28-2swm)

I. INTRODUCTION

The interplay between structural, electronic and magnetic degrees of freedom in cubic perovskites (of the form ABO_3) is crucial in understanding the emergence of various technologically relevant properties. One canonical example is that of colossal magnetoresistance (CMR), the property of a material to undergo large decreases of resistivity under the application of an external magnetic field. CMR emergence in the hole-doped perovskite manganites $\text{La}_{1-x}\text{Ca}_x\text{MnO}_3$ (LCMO) has been intensely studied over the past several decades, primarily due to its potential applications in novel data storage devices and sensor technologies [1]. Maximal decreases in the resistivity of LCMO (occurring at a composition $x = 3/8$) [2], are believed to be caused by percolative phase segregation between different insulating and metallic charge and orbital (dis)ordered states [3]. Hence, in order to optimize the CMR effect, and to appreciate how the different charge and orbital ordering phenomena control this property in these materials, it is imperative to obtain an accurate microscopic understanding

of these states, allowing one to successfully tune the properties in a targeted way.

However, the phase diagram of LCMO is ubiquitously complex [4,5], and many different control parameters are affected simultaneously upon Ca^{2+} doping that result in these different states. These effects include mixed Mn oxidation states, electronic band-narrowing phenomena, and different degrees of Jahn-Teller (JT) distortions and tolerance factor changes. All of these control parameters play a role in charge and orbital ordering. However, they also have a strong influence on the observed strain, domain structure and superstructure, and so it means that these competing complexities prevent an accurate microscopic understanding to determine to what extent each of these contribute to ordering phenomena, and hence the emergence and optimization of CMR.

The use of prototype systems allows one to overcome this competing complexity issue. In these systems, only one of the control parameters is allowed to vary systematically, while all of the others are in principle isolated as much as possible in an attempt to decouple these parameters from each other. This approach presents the opportunity to target how each type of complexity contributes independently to the emergence of charge and orbital ordering phenomena in manganite perovskites. For example, we have previously shown using cubic manganite quadruple perovskites $\text{AMn}_3\text{Mn}_4\text{O}_{12}$ ($A = \text{Ca}_{1-x}\text{Na}_x, \text{Hg}_{1-x}\text{Na}_x$), which decouple the $Pbnm$ structural degrees of freedom from the process of chemical doping, that for compositions of x giving an average Mn B site oxidation state coincident with compositions of LCMO of maximal

*Contact author: m.senn@warwick.ac.uk

CMR effects, a novel 1:3 orbital order:charge disorder striping occurs [6,7]. And, *via* the careful analysis of symmetry-breaking strain in the prototype systems $R_{\frac{5}{8}}\text{Ca}_{\frac{3}{8}}\text{MnO}_3$ (R = rare-earth cation) at this doping level, we have shown that the maximum in CMR coincides with the point of closest proximity to this novel orbital order:charge disorder state [8]. Hence, the use of prototype systems allows one to uncover crucial information regarding ordering phenomena which would otherwise not have been observed by considering the original LCMO solid solution.

The solid solution $\text{LaMn}_{1-x}\text{Ga}_x\text{O}_3$ (LMGO) proves to be another ideal prototype system for investigating the influence of the JT effect on orbital ordering phenomena in manganite perovskites, and specifically its interplay with strain that strongly affects any phase coexistence behavior. The solid solution end member LaMnO_3 is a canonical example of a material that exhibits long-range C -type orbital order [9]. In this case, the orbital order is caused by the cooperative JT effect, described as alternating directions of d_{z^2} orbitals within the orthorhombic $Pbnm$ a - b plane and layered along the c axis. Substitution of the JT-active high-spin Mn^{3+} cation for JT-inactive Ga^{3+} results in a reduction of the cooperative JT effect, which acts to reduce the magnitude or change the type of orbital order behavior. Using Ga^{3+} as the chosen substituent for high-spin Mn^{3+} is important because they both contain similar ionic radii in an octahedral environment: 0.645 Å for high-spin Mn^{3+} and 0.62 Å for Ga^{3+} [10]. This means additional octahedral rotations are minimized, isolating out tolerance factor effects as much as possible, while still retaining the orthorhombic $Pbnm$ structure of the insulating CMR-active LCMO phases.

The LMGO solid solution has previously been made and studied by both x-ray and neutron diffraction techniques to corroborate changes in orbital ordering behavior [11,12]. Lattice parameters of the $Pbnm$ orthorhombic unit cell converge from $b > a > c/\sqrt{2}$ to a pseudocubic state, where $b \approx a \approx c/\sqrt{2}$ at a range of Ga^{3+} substitution $0.5 < x < 0.6$. This same transition is observed in both the high-temperature phase transition of LaMnO_3 [13] and across the LCMO phase diagram at room temperatures [14]. Typically this is considered a fingerprint of orbital order-disorder behavior in manganite perovskites when using local structure probes of pair distribution function (PDF) [15,16]. Interestingly, an x-ray absorption spectroscopy study on LMGO points towards a displacive picture occurring instead of order-disorder [17]. Here, local JT distorted MnO_6 octahedra were found to become less distorted, but contain a large spread of Mn-O distances, as the substitution of Mn^{3+} for Ga^{3+} increases. Whether this phase transition concretely describes a displacive or order-disorder picture in LMGO is an interesting open question that should be studied by x-ray and neutron PDF. Nonetheless, while the orthorhombic to pseudocubic phase transition has been observed in LMGO, and its link to changes in magnetic behavior across the solid solution explained *via* orbital-mixing and orbital-flipping models [18,19], critical insight such as how each unique structural distortion of the $Pbnm$ perovskite system contributes to changes in orbital ordering, and the evolution of order parameters driving the pseudocubic state *via* experimental data, are missing from the literature.

Here, by careful Rietveld analysis of variable composition synchrotron x-ray and neutron powder diffraction data, employing the symmetry-adapted distortion mode formalism [20], we show that the trilinear coupling term ($\Gamma_5^+ M_2^+ M_3^+$) between shear strain, octahedral rotation, and the C -type orbital ordering mode acts as a driver for the orthorhombic to pseudocubic phase transition in LMGO. This transition is concomitant with orbital order-disorder transitions in manganite perovskites, and while it is controlled solely by a decrease of the M_3^+ mode amplitude towards zero in the LMGO system, our analysis reveals a second competitive coupling of the out-of-phase octahedral tilting mode (R_5^-) with the shear strain. To illustrate the generality of our results, we construct a function that describes the difference in Landau free energy between orbitally disordered and ordered states, and their associated shear strains, providing a tool to rationalize composition dependent trends in phase transition temperatures in these materials.

II. EXPERIMENT AND DATA ANALYSIS

$\text{LaMn}_{1-x}\text{Ga}_x\text{O}_3$ samples ($0 \leq x \leq 1$ in 0.1 increments) were prepared by the solid state synthesis method, using conditions adapted from Rao *et al.*, [21] with detailed synthesis conditions described in Supplemental Material [22] (see also Refs. [21,23–30] therein). Characterization of samples *via* synchrotron powder x-ray diffraction (PXRD) techniques was achieved using the high-resolution powder diffraction beamline I11 at the Diamond Light Source [31]. Data were collected at a temperature $T = 300$ K using the multi-analyser crystal detectors with an x-ray wavelength of $\lambda = 0.8259226(3)$ Å, as determined by refinement against an NIST Si standard. Samples were packed into 0.3 mm diameter borosilicate capillaries and data collected in Debye-Scherrer geometry. Compositions for $x = 0.2, 0.5, \text{ and } 0.7$ were characterized *via* powder neutron diffraction (PND) techniques using the high-resolution powder diffraction instrument D2B at the Institut Laue Langevin [32]. D2B data were collected at a wavelength of $\lambda = 1.59274(15)$ Å, as determined from refinement against an NAC standard, with datasets being obtained at a temperature $T = 300$ K [33]. Diffraction data were analyzed *via* the Rietveld refinement method using the software Topas Academic V7 [34].

Refinements were performed in the basis of irreducible representations (irreps), utilizing the symmetry-adapted formulation generated through the webtool ISODISTORT [20]. Structural distortions of a lower symmetry structure may be classified as transforming as irreps of its parent (aristotype) structure. In the case of the $Pbnm$ perovskite, unique structural distortions transform as eight different irreps with respect to the aristotype ABO_3 perovskite with a $Pm\bar{3}m$ space group and the A site chosen as the origin. These eight irreps, schematically shown in Fig. 1, are $R_4^-, R_5^-, X_5^-, M_2^+$, and M_3^+ which describe atomic displacements, and Γ_1^+, Γ_3^+ , and Γ_5^+ which describe unit cell strain. These irreps also contain an order parameter direction (OPD) that describes the directionality in which the distortion acts. It can be the case that multiple irreps with the same label but different OPD are present in a structural distortion. However, in the $Pbnm$ perovskites this is not the case and so specifying OPDs are not required. For more

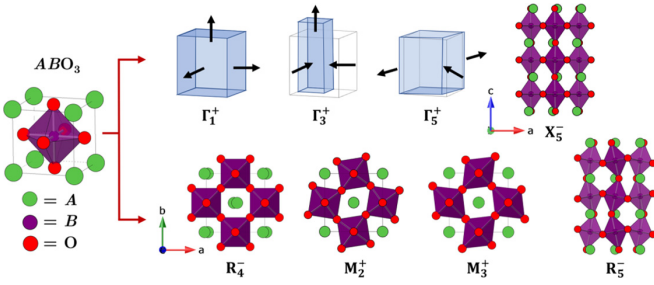


FIG. 1. Schematic of the character of eight irreps spanning the structural distortions of the $Pbnm$ ABO_3 perovskite with respect to the $Pm\bar{3}m$ aristotype. Purple shaded regions indicate the BO_6 octahedral environment. For distortion mode irreps R_4^- , R_5^- , X_5^- , M_2^+ , and M_3^+ the unit cell given is with respect to the $Pbnm$ space group. For strain irreps Γ_1^+ , Γ_3^+ , and Γ_5^+ the unshaded cell represents the undistorted $Pm\bar{3}m$ unit cell and the shaded cell represents the distorted unit cell. Arrows represent the direction of the unit cell distortion.

information the reader is directed towards the work of Senn and Bristowe [35]. Symmetry-mode analysis allows one to encapsulate orthogonal structural distortions as a single parameter that can be tracked as a function of different variables such as temperature, pressure and chemical composition. Their associated irreps allow one to determine symmetry-allowed coupling terms, constituting primary order parameters that drive phase transitions and emerging properties *via* the use of invariants analysis and Landau theory [36]. This is exemplified by the emergence of hybrid improper ferroelectricity in $Ca_3Mn_2O_7$ [37] and various magnetoelectric multiferroic couplings in perovskites [35]. Amplitudes of the distortion modes reported are given in terms of absolute A_p values, which refer to the aristotype-cell-normalized amplitude of a particular distortion. These have been given the symbol notation $Q(K_n^{+/-})$, where Q and $K_n^{+/-}$ denote the amplitude and specific irrep of the distortion, respectively. The latter provides information on the k point in the aristotype Brillouin zone (K), the enumeration number (n), and retention/violation of inversion symmetry of the distortion (+/-) with respect to the origin. This analysis facilitates a universal comparison to other perovskite material systems containing the same space group and referred to the same aristotype.

III. RESULTS AND DISCUSSION

Synchrotron PXRD and PND patterns show a high phase purity for each $LaMn_{1-x}Ga_xO_3$ sample across the solid solution (Figs. S1 and S2 [22]). Refinements of $Pbnm$ perovskite structural models against the data obtained show that lattice parameters produce the expected convergence behavior from $b > a > c/\sqrt{2}$ to $b \approx a \approx c/\sqrt{2}$ in the range $0.5 < x < 0.6$, indicating the orthorhombic to pseudocubic phase transition, consistent with the behavior reported in the literature (Table S1 and Fig. S3 [22]) [11,12]. Furthermore, the monotonic decrease of the unit cell volume as a function of x indicates that the stoichiometries of each element in each sample are consistent with the nominal stoichiometry, hence giving the successful formation of a solid solution (Fig. S4 [22]).

TABLE I. Fitted parameters of α and k for models describing Γ_5^+ evolution across the LMGO solid solution shown in Fig. 2(b). Estimated standard deviations for each refined parameter are given in parentheses.

Model	α	k
$\alpha M_2^+ M_3^+$	-29(1)	0
$\alpha M_2^+ M_3^+ + k$	-42.3(3)	0.605(12)

These initial results from the refinements indicate that no first-order phase transition between orthorhombic and pseudocubic phases, or segregation of phases, is observed, and that a continuous decrease in the magnitude of long-range C -type orbital order, and hence the cooperative JT effect, occurs. This continuous character of the phase transition between orthorhombic (JT-ordered) and pseudocubic (non-JT ordered) is in agreement with previous XAS studies in literature [17].

A number of effects that obfuscate obtaining insight into the nature of the orthorhombic to pseudocubic phase transition are minimized by studying LMGO. One includes thermal effects since the transition occurs at much lower temperatures compared to the equivalent temperature-dependent transition in $RMnO_3$ [27,38]. This means that dynamic disorder effects are significantly reduced in comparison, and static disorder effects become more prevalent and are easier to discriminate. Another is that of B site disorder, similar to the A site disorder effects studied in magnetoresistive manganite perovskites [39,40]. However, for the B site size variances σ^2 for each LMGO, calculated in a similar manner to the A site variance equivalents, even the largest value of σ^2 , occurring for $x = 0.5$, is $\approx 1.6 \times 10^{-4} \text{ \AA}^2$, which is an order of magnitude smaller than the smallest σ^2 compositions studied by Rodríguez-Martínez *et al.* [39,40]. Hence, B site disorder effects are considered negligible in LMGO compared to the changes in JT distortions.

Distortion mode amplitudes for the irreps that describe the out-of-phase and in-phase BO_6 octahedral rotations, R_5^- and M_2^+ respectively, and the cooperative JT distortion, M_3^+ , across the LMGO solid solution are shown in Fig. 2(a). The full set of distortion modes is shown in Figs. S5–S11. For M_3^+ a large decrease is observed, as expected, due to the systematic reduction of JT-active components across the solid solution. When compositions of the solid solution reach $x \approx 0.5/0.6$, where the orthorhombic to pseudocubic phase transition takes place, the amplitude of M_3^+ remains nonzero. This indicates that the C -type orbital order distortion extends beyond the percolation threshold of a JT long B -O bond within the perovskite lattice. As noted by Zhou and Goodenough [41], intrinsic octahedral distortions of this kind manifest themselves even for JT-inactive perovskites, such as $LaGaO_3$, which are imposed by the two unique BO_6 octahedral rotations. Therefore, it is expected to have a small, nonzero value to M_3^+ even for the pseudocubic phases within the LMGO solid solution. These octahedral rotation structural distortions themselves are able to generate the $Pbnm$ perovskite structure [42], and a further discussion on this in terms of symmetry-allowed coupling terms of irreps is presented later.

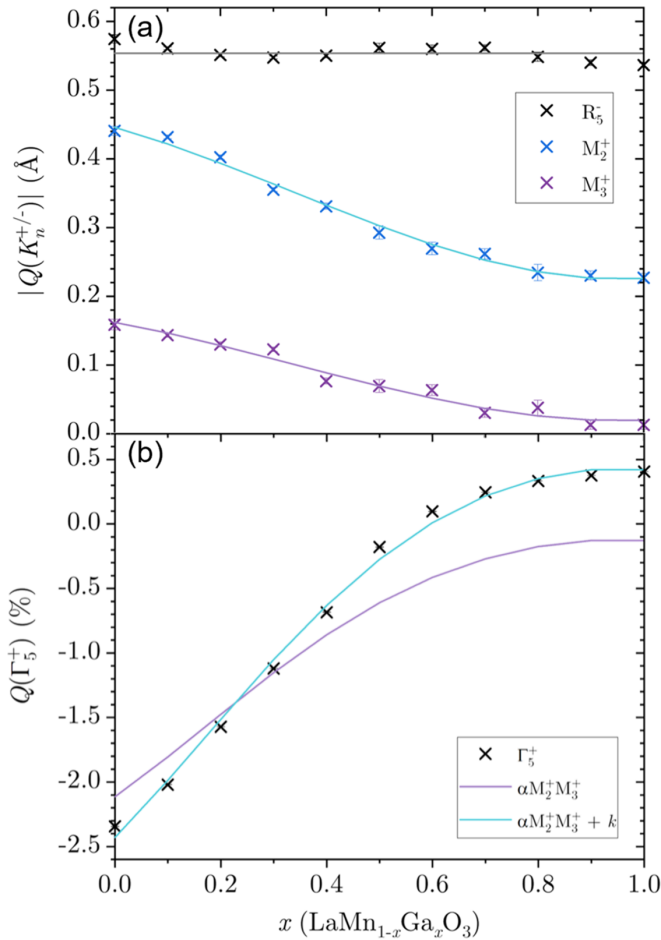


FIG. 2. (a) Distortion mode amplitudes of structural distortions that transform as the irreps R_5^- , M_2^+ , and M_3^+ of the $Pbnm$ perovskite across the LMGO solid solution. (b) Variation of the shear strain irrep Γ_5^+ across the LMGO solid solution. Each dataset is fit, informed by the invariant analysis as described in the text. Further details and fitting coefficients are given in Figs. S9–S11 [22]. Two models are fit for conditions of $k = 0$ (purple line) and $k \neq 0$ (blue line). Fitted parameters in these models are given in Table I.

The amplitude of the in-phase octahedral rotation acting about the $Pbnm$ c axis, M_2^+ , is observed to decrease in a similar rate to that of M_3^+ , whereas the out-of-phase octahedral rotation acting along the b axis, R_5^- , is observed to remain essentially unaffected across the solid solution. The differing evolution of the unique octahedral rotation modes show that the complexity of tolerance factor effects are minimized in LMGO. If there were significant tolerance factor effects occurring in this system, despite the minor differences in high-spin Mn^{3+} and Ga^{3+} ionic radii, then R_5^- would be expected to decrease more significantly and at a similar rate to M_2^+ . To corroborate this point, the concomitant changes of R_5^- , M_2^+ and M_3^+ mode amplitudes for reported structural data at $T = 300$ K of the series of $Pbnm$ manganite perovskites $R^{3+}MnO_3$ ($R^{3+} = \text{rare-earth cation}$) [23–28] are plotted as a function of tolerance factor (Fig. S12 [22]). In this series, tolerance factor effects are demonstrated by the significant changes in the A site ionic radius. This therefore indicates that there is some intrinsic coupling between M_2^+ and M_3^+

distortion modes, which act as primary order parameters in the Landau free energy of the LMGO system describing the orthorhombic to pseudocubic phase transition.

Further examining the relationship between these three distortion modes, each is fitted against polynomial functions of x to capture a model describing the variation of each across the LMGO solid solution. The fitting of R_5^- is achieved by approximating its variation with a single constant $a_{R_5^-}$, with any potential changes in amplitude across the series deviating only 5% of the average value, determined as $0.554(2)$ Å. Highlighting the similar evolution of M_2^+ and M_3^+ distortions, both are fit to a third-order polynomial function of the form: $y = a + bx + cx^2 + dx^3$. Values of a were allowed to be refined and independent of each other for both datasets (written as $a_{M_2^+}$ and $a_{M_3^+}$). To account for the different scaling of M_2^+ and M_3^+ amplitudes, a refined scaling factor was added to the coefficients of x (b , c and d), with these coefficients being refined simultaneously against both M_2^+ and M_3^+ datasets, to produce a refined scaling factor of $1.54(9)$. The resulting coefficients of each polynomial are given in Figs. S9–S11 [22]. This choice is made due to the linear dependence of M_2^+ and M_3^+ distortions between each other, as demonstrated by the linearity exhibited by M_2^+ versus M_3^+ plots shown in Fig. S13 [22]. A third-order polynomial function is chosen here as a result of fitting the lowest order polynomial that gives the best quality of fit to the data. In consideration as to why these two primary order parameters couple so strongly together, we note that it was determined by Varignon *et al.* studying $A^{3+}V^{3+}O_3$ perovskites that the sum of two symmetry-allowed trilinear coupling terms $R_5^- X_5^- M_2^+ + R_5^- X_5^- M_3^+$ acts to lower the Landau free energy of these systems [43]. In our LMGO solid solution, we may assume R_5^- , M_2^+ , and M_3^+ as the only primary order parameters, allowing X_5^- to be written as $\approx \alpha R_5^- M_2^+$, and noting R_5^- is constant for this system (k), then the trilinear term reduces to $k((M_2^+)^2 + M_2^+ M_3^+)$ producing the observed linear dependence of BO_6 rotation and JT modes on each other. Alternatively this fact may be appreciated by considering the experimentally observed evolution of X_5^- , which given the constant value of R_5^- means a linear dependence with both M_2^+ and M_3^+ (see Fig. S8 [22]).

Invariants analysis allows one to identify various coupling schemes between order parameters that can naturally occur in the Landau free energy of a phase transition of a system. In the present case, the transition we consider is the hypothetical phase transition from $Pm\bar{3}m$ to $Pbnm$ perovskite structures. Generally those that have the greatest effect on the Landau free energy are the lowest order terms. Hence, in the following analysis, we only consider terms up to the third and fourth order. By using the webtool INVARIANTS in the ISOTROPY package [44], a variety of third and fourth-order terms are found. However, we highlight a single trilinear coupling term of $\Gamma_5^+ M_2^+ M_3^+$ which couples both the in-phase octahedral rotation and JT distortion to shear unit cell strain as it is the only trilinear term with respect to, what we consider to be, the primary order parameters R_5^- , M_2^+ , and M_3^+ that is allowed by symmetry. The rationale for this choice of primary order parameters is that the $Pbnm$ perovskite space group can be solely generated from the irreps R_5^- and M_2^+ , and that we systematically tune the amplitude of M_3^+ modes in the LMGO

solid solution by substitution of JT-active cations (Mn^{3+}) for non JT-active cations (Ga^{3+}). Hence, order parameters transforming as these three irreps are the only ones considered. While the existence of this coupling term has been commented on in previous literature [42,45,46], as far as we are aware there are no reported experimental data that show how the amplitude of this, or components of this term, varies as a function of the LMGO solid solution. Schmitt *et al.* demonstrate that neither a single octahedral rotation M_2^+ or shear strain Γ_5^+ can lift the degeneracy of the six Mn-O bonds to produce the M_3^+ distortion, but that the combined action of both is required to induce nonzero M_3^+ [45]. These findings then indicate that this trilinear term is a primary driver of the orthorhombic-pseudocubic phase transition in LMGO, and in *Pbnm* manganite perovskites in general. This is regardless of whether locally a displacive mechanism, suggested by x-ray absorption spectroscopy in LMGO [17], or an order-disorder mechanism, as observed generally in *Pbnm* manganite perovskites [15,16], conclusively occurs.

Having identified the significance of this trilinear coupling term, we show in Fig. 2(b) the variation of the shear unit cell strain Γ_5^+ across the solid solution. Γ_5^+ decreases in amplitude towards zero at a point for $x \approx 0.5/0.6$, where for LMGO with larger x , Γ_5^+ remains positive and close to zero. The alleviation of shear strain here demonstrates a symmetry-based fingerprint of the transition from orthorhombic to pseudocubic states, and hence orbital order to disorder behavior. By considering the trilinear coupling term $\Gamma_5^+ M_2^+ M_3^+$, shear strain data is fit to functions of the form $\alpha M_2^+ M_3^+ + k$, where components of M_2^+ and M_3^+ are taken as the third-order polynomials of x , as determined in Fig. 2, and α and k are refined. The results of this fitting procedure are given in Table I. The fits show that $\alpha M_2^+ M_3^+$ with k set to zero captures the same kind of general trend as observed experimentally, but it does not fit the data adequately. This means that models which only assume active distortions of M_2^+ and M_3^+ are not accurate enough by themselves, and hence require extra degrees of complexity to the model. Allowing the value of k to vary from zero results in a much improved fit. In this case, k accounts for the presence of other structural distortions that manifest across the solid solution, and in the case of the *Pbnm* perovskite it is most likely the action of the second unique octahedral rotation R_5^- via the linear-quadratic term $\Gamma_5^+ (R_5^-)^2$. Since R_5^- does not vary significantly across the LMGO solid solution, the effect of this coupling ($\beta = k/(R_5^-)^2$) is well approximated by a constant background contribution to the shear strain. Hence, we demonstrate the large degree of coupling between M_2^+ and M_3^+ , which captures the transition from orthorhombic to pseudocubic states *via* the trilinear coupling term $\Gamma_5^+ M_2^+ M_3^+$.

With the culmination of all of the presented crystallographic data here, it appears possible that the LMGO solid solution can act as an ideal system to trace how JT distortions tune the orthorhombic-pseudocubic phase transition in *Pbnm* manganite perovskites. To understand the local ordering that gives rise to the crystallographically observed average structural distortions, we perform a series of Monte Carlo (MC) simulations (see Fig. 3). We consider two-dimensional simulations of 10×10 arrays of corner-sharing rhombuses. Each rhombus is assigned randomly as JT-active or JT-inactive

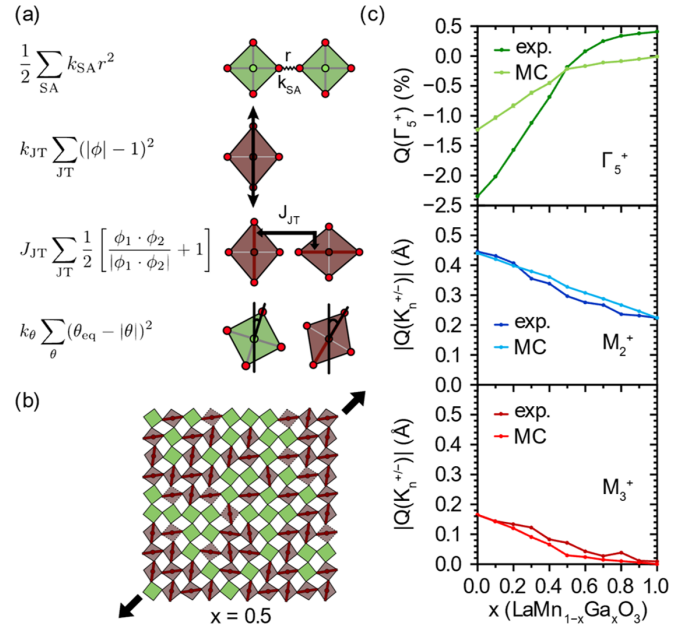


FIG. 3. Results from two-dimensional Monte Carlo (MC) simulations on $\text{LaMn}_{1-x}\text{Ga}_x\text{O}_3$. (a) Energy penalties used in the MC simulation. (b) A representative relaxed configuration for $x = 0.5$, showing longer range order at the percolation threshold for JT long bonds. (c) The evolution of the M_3^+ , M_2^+ , and Γ_5^+ modes extracted from the relaxed MC simulations.

subject to a predefined overall composition x . These rhombuses approximate the cross-section of corner-sharing MnO_6 and GaO_6 octahedra. Each rhombus has four degrees of freedom: its horizontal and vertical position, its tilt angle θ , and a JT distortion magnitude ϕ . The equilibrium value of θ for a JT-active and a JT-inactive rhombus were obtained from the corresponding tilts in the end members LaMnO_3 and LaGaO_3 respectively. The value of ϕ was set to zero for every rhombus assigned as JT-inactive, and allowed to vary with an equilibrium magnitude of 1 for rhombuses assigned as JT active. The actual rhombic distortion given by $\phi = 1$ was set to mimic the JT distortion magnitude observed in LaMnO_3 itself. The Monte Carlo energy term contained four terms: (i) a split-atom term [47], which acts to maintain sensible connectivity of neighboring rhombuses, (ii) a JT term which penalized departures from ideal JT distortion geometries for JT-active sites, (iii) a JT coupling term that favored alternation of JT distortion axes, and (iv) a tilt term that penalized departures from the ideal tilt angle (for a given composition). The spring constants assigned to these various terms [see Fig. 3(a)] were varied to ensure sensible convergence of the MC simulations; their absolute values did not affect the ground-state structures that emerged. Full details of the implementation of our MC simulations are given in Supplemental Material [22].

In a first set of simulations, we did not allow geometric relaxation of the box, and hence the shear strain was identically zero. These initial simulations did capture a degree of coupling between the average tilt and rotation observed as a function of x , but it is clear from their high residual ground state energies that they are highly strained. Consequently we

repeated these simulations whilst allowing the simulation box to shear (i.e., it may itself become a rhombus). For values of x less than about 0.5, this additional degree of freedom serves to reduce the residual ground state energy significantly, producing results where the majority of rhombuses are able to satisfy their preferred local geometry [see Fig. 3(b) for $x = 0.5$]. It is important to note that this shearing arises spontaneously from our simple Hamiltonian that captures only the desire for the rhombuses to rotate and distort and should hence be thought of as the microscopic origin behind the trilinear terms $\Gamma_5^+ M_2^+ M_3^+$ that we and others have identified through invariants analysis. In particular, there was no explicit term involving shear in the MC Hamiltonian.

Our simulations produce configurations that exhibit long-range orbital ordering from $x = 0$ right up to $x = 0.5$ which is the theoretical JT bond percolation limit in a square lattice. Next we collapse our microscopic simulations down to create an average $Pbnm$ unit cell from which we analyze the evolution of the M_3^+ , M_2^+ , and Γ_5^+ mode amplitudes [Fig. 3(c)]. The average evolution of M_3^+ and M_2^+ is in excellent agreement with those observed in our crystallographic study up to $x = 0.5$. Beyond that the MC simulation undergoes a phase transition to an orbitally disordered state. On the other hand, our diffraction data evidence a continuous evolution as a function of x . The discrepancy is because the shear strain (Γ_5^+) only arises in our MC simulations as a consequence of long-range coupling between M_3^+ and M_2^+ , while in a real $Pbnm$ perovskite, it is ever-present through the coupling to the out-of-phase BO_6 tilt ($\Gamma_5^+ (R_5^-)^2$) that is necessarily ignored in our two-dimensional simulations. Indeed, the evolution of Γ_5^+ [Fig. 3(c)] has a similar trend as our experimental model in which we ignored the constant term arising from the coupling to R_5^- [Fig. 2(b)].

The present results therefore strongly suggest that far from the shear strain tending to zero (i.e., the occurrence of the pseudocubic state) being a symptom of orbital disorder in other systems, it is more likely to be a cause. For example, perovskite systems adopting shear strain states that are predisposed to a strong coupling between M_3^+ and M_2^+ will tend to exhibit orbital ordering even below the percolation threshold. On the other hand, in a perovskite that is highly resistant to shearing in the correct manner, long-range orbital order will be suppressed even above the percolation threshold. The lowest order term in the Landau free energy, in the absence of any JT activity, that couples shear strain to the internal structural degrees of freedom, is $\Gamma_5^+ (R_5^-)^2$. It is therefore interesting to explore the relationship between the shear strain state observed as a function of out-of-phase octahedral rotations R_5^- and the amplitude of M_3^+ , the C-type orbital ordering mode (Fig. 4). We note that the former has a strong correlation with temperature and tolerance factor (see Supplemental Material [22]) but not with the concentration of JT-active species which is instead strongly correlated with the latter only (i.e., see Fig. 2). To reflect this situation, we consider the following contribution of the second- and third-order terms only to the Landau free energy, \mathcal{F} , associated with the orbital disorder to order transition: $\mathcal{F} = \alpha Q_{\Gamma_5^+} Q_{M_3^+} Q_{M_2^+} + \beta Q_{\Gamma_5^+} (Q_{R_5^-})^2 + \gamma (Q_{\Gamma_5^+})^2 + \delta (Q_{M_3^+})^2$, i.e., we aim to capture the essential energy difference between these phases. We note

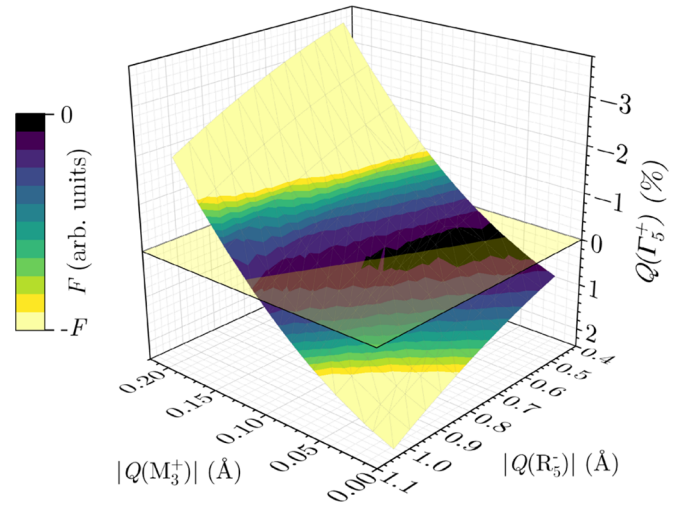


FIG. 4. 3D surface showing the shear strain values obtained by minimizing the Landau free energy expression described in the text. The Jahn-Teller distortion M_3^+ and the octahedral rotation R_5^- are treated as independent variables for this purpose. The surface is color coded according to the Landau energy associated with a minimum energy surface. Regions about the plotted plane $\Gamma_5^+ = 0$ indicate the pseudocubic state.

also that we do not include quartic bounding terms for M_3^+ and R_5^- since we will take them as the independent variables in the analysis that follows. Taking the differential of the above function with respect to Γ_5^+ , under the additional assumption that we may write $Q_{M_2^+} = 1.5Q_{M_3^+} + 0.2$ (see Fig. S13), gives the energy surface associated with the Γ_5^+ values that is a dependent variable of M_3^+ and R_5^- (Fig. 4). We note that the values of α and β are constrained *via* our fits reported in Table I, and γ is chosen such that the minimum values of Γ_5^+ are scaled appropriately to the experimental data. The gain in the Landau free energy associated with orbital order is captured by δ , and we assume this to be proportional to $Q_{M_3^+}$ which itself is proportional to the concentration of JT active species. The choice of δ has no effect on the function describing the energy surface, it merely provides an offset to the Landau Free energy (which is in arbitrary units) plotted on the surface.

By construction, the intersection of this surface with the plane $\Gamma_5^+ = 0$ must result in a contribution to this Landau Free energy expression that is only dependent on $\delta (Q_{M_3^+})^2$. However, there are several nontrivial features evident in this energy surface. Firstly, it is clear to see that $\Gamma_5^+ = 0$ is not realized for a fixed M_3^+ value (i.e., fixed JT concentration), but rather for a fixed relationship with the out-of-phase tilt amplitude $Q_{R_5^-} = \sqrt{((-\alpha/\beta)(1.5(Q_{M_3^+})^2 + 0.2Q_{M_3^+}))}$. Secondly, the energy surface maxima (i.e., least stable and closest to $\mathcal{F} = 0$) are higher and much shallower about trajectories taken through the plane at lower fixed tilt amplitude ($Q_{R_5^-}$) values than at higher ones. This simple model then explains why orbital disorder phase transitions are pushed to much higher temperatures in $RMnO_3$ with a decreasing ionic radius of R , which have low tolerance factors and hence high R_5^- even at elevated temperatures [27,38]. Taken together our

simple model is suggestive that the pseudocubic state arises when a cancellation between contributions from energy terms involving $Q_{R_5^-}$ and $Q_{M_3^+}$ in \mathcal{F} would occur. Or put another way, our Landau free energy expression implies that specific strain states are a cause of the orbital order-disorder phenomena rather than a symptom.

Finally, we note that we have not explicitly dealt with the role of the tetragonal-type Γ_3^+ strain. Schmitt *et al.* undertook an analysis of the lowering of the Landau free energy in manganite perovskites, with respect to their unique structural distortions in the basis of irreps, *via* DFT calculations on the system LaMnO_3 [45]. In their study, they focus on the origin of the joint high-temperature metal-to-insulator and orbital order transition which occurs at $T = 750$ K, and also on the stability of different magnetic phases. Through their calculations, they find that the action of compressive tetragonal strain ($-\Gamma_3^+$) stabilizes the *A*-type antiferromagnetic (AFM) state over a ferromagnetic (FM) one while also producing a lower potential energy well for an insulating orbitally ordered state over a metallic one. We observe some subtle deviation of the tetragonal strain Γ_3^+ from a linear fit in M_3^+ and M_2^+ (see Fig. S5 [22]), particularly at high x where a crossover from AFM *A*-type to FM occurs [12] that would seem to support the idea of Schmitt *et al.* that there is also a strong degree of coupling of electron and spin correlations, with the M_3^+ and M_2^+ modes.

IV. CONCLUSION

We have shown that the orthorhombic to pseudocubic phase transition in $\text{LaMn}_{1-x}\text{Ga}_x\text{O}_3$ (LMGO) can be described as being driven by a trilinear coupling term $\Gamma_5^+ M_2^+ M_3^+$ in the Landau free energy. Our Monte Carlo (MC) simulations produce configurations consistent with *C*-type orbital order up to the JT bond percolation threshold ($x = 0.5$), only if the system is allowed to relax under macroscopic shear strain, revealing

the microscopic origin of this coupling term. While our MC simulations show a well-defined transition to an orbitally disordered state at $x = 0.5$, the more continuous evolution in our experimental data reveals a second, competitive coupling of the shear strain Γ_5^+ with the out-of-phase octahedral tilting R_5^- . This observation motivated us to construct a function that describes the difference in Landau free energy between orbitally disordered and ordered states, which explains the observations that RMnO_3 , with high degrees of octahedral tilting, have their orbital disorder transitions pushed to higher temperatures. Our results point to the fact that the pseudocubic state in *Pbnm* manganite perovskites should be viewed as a cause rather than a symptom of orbital disorder, and thus they have relevance for the control of rich electronic and magnetic properties of perovskites which have orbital degrees of freedom.

ACKNOWLEDGMENTS

B.R.M.T. thanks the University of Warwick and the EPSRC for studentship and funding (EP/R513374/1) and M.S.S. acknowledges the Royal Society for a fellowship (UF160265 & 231012). The initial sample characterization to assess phase purity was performed via the Warwick X-ray Research Technology Platform. We are grateful to the STFC for the provision of synchrotron beam time at I11, Diamond Light Source, under the block allocation grant award (CY32893), and to the ILL for neutron beam time at D2B under the proposal number 5-24-693 (DOI: [10.5291/ILL-DATA.5-24-693](https://doi.org/10.5291/ILL-DATA.5-24-693)). A.L.G. gratefully acknowledges financial support from the E.R.C. (Advanced Grant 788144), and the S.T.F.C. (studentship to E.A.H.).

DATA AVAILABILITY

The data that support the findings of this article are openly available [22,33].

-
- [1] A. P. Ramirez, Colossal magnetoresistance, *J. Phys.: Condens. Matter* **9**, 8171 (1997).
 - [2] S. W. Cheong and H. Y. Hwang, in *Colossal Magnetoresistance Oxides*, edited by Y. Tokura (Gordon and Breach, London, 2000), Chap. 7.
 - [3] M. Uehara, S. Mori, C. H. Chen, and S.-W. Cheong, Percolative phase separation underlies colossal magnetoresistance in mixed-valent manganites, *Nature (London)* **399**, 560 (1999).
 - [4] P. Schiffer, A. P. Ramirez, W. Bao, and S.-W. Cheong, Low temperature magnetoresistance and the magnetic phase diagram of $\text{La}_{1-x}\text{Ca}_x\text{MnO}_3$, *Phys. Rev. Lett.* **75**, 3336 (1995).
 - [5] M. Fäth, S. Freisem, A. A. Menovsky, Y. Tomioka, J. Aarts, and J. A. Mydosh, Spatially inhomogeneous metal-insulator transition in doped manganites, *Science* **285**, 1540 (1999).
 - [6] W.-T. Chen, C.-W. Wang, C.-C. Cheng, Y.-C. Chuang, A. Simonov, N. C. Bristowe, and M. S. Senn, Striping of orbital-order with charge-disorder in optimally doped manganites, *Nat. Commun.* **12**, 6319 (2021).
 - [7] B. R. M. Tragheim, S. Simpson, E.-P. Liu, M. S. Senn, and W.-T. Chen, Intrinsic electronic phase separation and competition between *G*-type, *C*-type, and *CE*-type charge and orbital ordering modes in $\text{Hg}_{1-x}\text{Na}_x\text{Mn}_3\text{Mn}_4\text{O}_{12}$, *Phys. Rev. B* **110**, 245123 (2024).
 - [8] B. R. M. Tragheim, C. Ritter, and M. S. Senn, Proximity to a state with orbital order and charge disorder in optimally doped $\text{R}_{5/8}\text{Ca}_{3/8}\text{MnO}_3$ perovskites, *Phys. Rev. B* **110**, 235141 (2024).
 - [9] J. B. Goodenough, Theory of the role of covalence in the perovskite-type manganites [$\text{La}, M(\text{II})$] MnO_3 , *Phys. Rev.* **100**, 564 (1955).
 - [10] R. D. Shannon, Revised effective ionic radii and systematic studies of interatomic distances in halides and chalcogenides, *Acta Crystallogr. Sect. A: Found. Adv.* **32**, 751 (1976).
 - [11] J. B. Goodenough, A. Wold, R. J. Arnett, and N. Menyuk, Relationship between crystal symmetry and magnetic

- properties of ionic compounds containing Mn^{3+} , *Phys. Rev.* **124**, 373 (1961).
- [12] J. Blasco, J. García, J. Campo, M. C. Sánchez, and G. Subías, Neutron diffraction study and magnetic properties of $\text{LaMn}_{1-x}\text{Ga}_x\text{O}_3$, *Phys. Rev. B* **66**, 174431 (2002).
- [13] P. Norby, I. G. K. Andersen, E. K. Andersen, and N. H. Andersen, The crystal structure of Lanthanum Manganate (III), LaMnO_3 , at room temperature and at 1273 K under N_2 , *J. Solid State Chem.* **119**, 191 (1995).
- [14] B. B. Van Aken, O. D. Jurchescu, A. Meetsma, Y. Tomioka, Y. Tokura, and T. T. M. Palstra, Orbital-order-induced metal-insulator transition in $\text{La}_{1-x}\text{Ca}_x\text{MnO}_3$, *Phys. Rev. Lett.* **90**, 066403 (2003).
- [15] P. M. M. Thygesen, C. A. Young, E. O. R. Beake, F. D. Romero, L. D. Connor, T. E. Proffen, A. E. Phillips, M. G. Tucker, M. A. Hayward, D. A. Keen, and A. L. Goodwin, Local structure study of the orbital order/disorder transition in LaMnO_3 , *Phys. Rev. B* **95**, 174107 (2017).
- [16] X. Qiu, T. Proffen, J. F. Mitchell, and S. J. L. Billinge, Orbital correlations in the pseudocubic O and rhombohedral R phases of LaMnO_3 , *Phys. Rev. Lett.* **94**, 177203 (2005).
- [17] M. C. Sánchez, G. Subías, J. García, and J. Blasco, Stability of the tetragonal Mn^{3+}O_6 distortions in the $\text{LaMn}_{1-x}\text{Ga}_x\text{O}_3$ series by x-ray absorption spectroscopy, *Phys. Rev. B* **69**, 184415 (2004).
- [18] J.-S. Zhou and J. B. Goodenough, Orbital mixing and ferromagnetism in $\text{LaMn}_{1-x}\text{Ga}_x\text{O}_3$, *Phys. Rev. B* **77**, 172409 (2008).
- [19] J. Farrell and G. A. Gehring, Interplay between magnetism and lattice distortions in $\text{LaMn}_{1-x}\text{Ga}_x\text{O}_3$, *New J. Phys.* **6**, 168 (2004).
- [20] B. J. Campbell, H. T. Stokes, D. E. Tanner, and D. M. Hatch, ISODISPLACE: a web-based tool for exploring structural distortions, *J. Appl. Crystallogr.* **39**, 607 (2006).
- [21] G. H. Rao, J. R. Sun, K. Bärner, and N. Hamad, Crystal structure and magnetoresistance of Na-doped LaMnO_3 , *J. Phys.: Condens. Matter* **11**, 1523 (1999).
- [22] See Supplemental Material at <http://link.aps.org/supplemental/10.1103/cj28-2swm> for synthesis conditions of LMGO, Rietveld refinement profiles of PXRD and PND data, crystallographic data of $Pbnm$ LMGO structural models, extracted strain and distortion modes fit with polynomial functions and their coefficients, strain and distortion modes of various published $A^{3+}\text{MnO}_3Pbnm$ structural models at 300 K, $|Q(\text{M}_2^+)|$ versus $|Q(\text{M}_3^+)|$ plot, full details of Monte Carlo simulations, folder containing CIFs of LMGO structural models, and folder containing raw synchrotron PXRD and PND datasets collected.
- [23] J. Rodríguez-Carvajal, M. Hennion, F. Moussa, L. Pinsard A. H. Moudden, and A. Revcolevschi, Neutron-diffraction study of the Jahn-Teller transition in stoichiometric LaMnO_3 , *Phys. Rev. B* **57**, R3189(R) (1998).
- [24] Z. Jiráček, J. Hejtmanek, K. Knížek, and R. Sonntag, Structure and properties of the $\text{Pr}_{1-x}\text{K}_x\text{MnO}_3$ perovskites ($x = 0-0.15$), *J. Solid State Chem.* **132**, 98 (1997).
- [25] J. A. Alonso, M. J. Martínez-Lope, M. T. Casais, and M. T. Fernández-Díaz, Evolution of the Jahn-Teller distortion of MnO_6 octahedra in RMnO_3 perovskites ($R = \text{Pr, Nd, Dy, Tb, Ho, Er, Y}$): a neutron diffraction study, *Inorg. Chem.* **39**, 917 (2000).
- [26] D. O'Flynn, C. V. Tomy, M. R. Lees, A. Daoud-Aladine, and G. Balakrishnan, Multiferroic properties and magnetic structure of $\text{Sm}_{1-x}\text{Y}_x\text{MnO}_3$, *Phys. Rev. B* **83**, 174426 (2011).
- [27] B. Dabrowski, S. Kolesnik, A. Baszczuk, O. Chmaissem, T. Maxwell, and J. Mais, Structural, transport, and magnetic properties of RMnO_3 perovskites ($R = \text{La, Pr, Nd, Sm, }^{153}\text{Eu, Dy}$), *J. Solid State Chem.* **178**, 629 (2005).
- [28] M. Tachibana, T. Shimoyama, H. Kawaji, T. Atake, and E. Takayama-Muromachi, Jahn-Teller distortion and magnetic transitions in perovskite RMnO_3 ($R = \text{Ho, Er, Tm, Yb, and Lu}$), *Phys. Rev. B* **75**, 144425 (2007).
- [29] N. Metropolis, A. W. Rosenbluth, M. N. Rosenbluth, A. H. Teller, and E. Teller, Equation of state calculations by fast computing machines, *J. Chem. Phys.* **21**, 1087 (1953).
- [30] D. P. Landau and K. Binder, *A Guide to Monte Carlo Simulations in Statistical Physics* (Cambridge University Press, Cambridge, 2015).
- [31] S. P. Thompson, J. E. Parker, J. Potter, T. P. Hill, A. Birt, T. M. Cobb, F. Yuan, and C. C. Tang, Beamline I11 at Diamond: A new instrument for high resolution powder diffraction, *Rev. Sci. Instrum.* **80**, 075107 (2009).
- [32] A. W. Hewat, D2B, a new high resolution neutron powder diffractometer at ILL Grenoble, *Mater. Sci. Forum* **9**, 69 (1986).
- [33] M. S. Senn, C. Crawford, C. Ritter, S. Simpson, and B. Tragheim, Interplay of Jahn-Teller distortions and orbital order with lattice and local modes in $\text{LaMn}_{1-x}\text{Ga}_x\text{O}_3$ (Institut Laue-Langevin (ILL), 2023), doi:[10.5291/ILL-DATA.5-24-693](https://doi.org/10.5291/ILL-DATA.5-24-693).
- [34] A. A. Coelho, TOPAS and TOPAS-Academic: an optimization program integrating computer algebra and crystallographic objects written in C++, *J. Appl. Crystallogr.* **51**, 210 (2018).
- [35] M. S. Senn and N. C. Bristowe, A group-theoretical approach to enumerating magnetoelectric and multiferroic couplings in perovskites, *Acta Crystallogr. Sect. A: Found. Adv.* **74**, 308 (2018).
- [36] Edited by D. Ter Haar, On the theory of phase transitions, *Collected Papers of L. D. Landau* (Pergamon, 1965), pp. 193–216.
- [37] N. A. Benedek and C. J. Fennie, Hybrid improper ferroelectricity: a mechanism for controllable polarization-magnetization coupling, *Phys. Rev. Lett.* **106**, 107204 (2011).
- [38] J.-S. Zhou and J. B. Goodenough, Orbital order-disorder transition in single-valent manganites, *Phys. Rev. B* **68**, 144406 (2003).
- [39] L. M. Rodríguez-Martínez and J. P. Attfield, Cation disorder and size effects in magnetoresistive manganese oxide perovskites, *Phys. Rev. B* **54**, R15622 (1996).
- [40] L. M. Rodríguez-Martínez, H. Ehrenberg, and J. P. Attfield, Disorder effects on structural and electronic transitions in high tolerance factor manganite perovskites, *Solid State Sci.* **2**, 11 (2000).
- [41] J.-S. Zhou and J. B. Goodenough, Intrinsic structural distortion in orthorhombic perovskite oxides, *Phys. Rev. B* **77**, 132104 (2008).
- [42] M. A. Carpenter and C. J. Howard, Symmetry rules and strain/order-parameter relationships for coupling between octahedral tilting and cooperative Jahn-Teller transitions in ABX_3

- perovskites. I. Theory, *Acta Crystallogr. Sect. B: Struct. Sci. Cryst. Eng. Mater.* **65**, 134 (2009).
- [43] J. Varignon, N. C. Bristowe, E. Bousquet, and P. Ghosez, Coupling and electrical control of structural, orbital and magnetic orders in perovskites, *Sci. Rep.* **5**, 15364 (2015).
- [44] D. M. Hatch and H. T. Stokes, INVARIANTS: program for obtaining a list of invariant polynomials of the order-parameter components associated with irreducible representations of a space group, *J. Appl. Crystallogr.* **36**, 951 (2003).
- [45] M. M. Schmitt, Y. Zhang, A. Mercy, and P. Ghosez, Electron-lattice interplay in LaMnO_3 from canonical Jahn-Teller distortion notations, *Phys. Rev. B* **101**, 214304 (2020).
- [46] G. G. Guzmán-Verri, R. T. Brierley, and P. B. Littlewood, Cooperative elastic fluctuations provide tuning of the metal-insulator transition, *Nature (London)* **576**, 429 (2019).
- [47] A. P. Giddy, M. T. Dove, G. S. Pawley, and V. Heine, The determination of rigid-unit modes as potential soft modes for displacive phase transitions in framework crystal structures, *Acta Crystallogr. Sect. A: Found. Adv.* **49**, 697 (1993).